5-22-2017

Chain length effect on the structure and stability of antimicrobial peptides of the (RW)n series

Nsoki Phambu
Tennessee State University

Bashiyar Almarwani
Tennessee State University

Arlette M. Garcia
Tennessee State University

Nafisa S. Hamza
Tennessee State University

Amira Muhsen
Xavier University of Louisiana

See next page for additional authors

Recommended Citation
Nsoki Phambu, Bashiyar Almarwani, Arlette M. Garcia, Nafisa S. Hamza, Amira Muhsen, Jacqueline E. Baidoo, Anderson Sunda-Meya, "Chain length effect on the structure and stability of antimicrobial peptides of the (RW)n series", Biophysical Chemistry, Volume 227, 2017, Pages 8-13, ISSN 0301-4622, https://doi.org/10.1016/j.bpc.2017.05.009.

Chain length effect on the structure and stability of antimicrobial peptides of the $(RW)_n$ series

Nsoki Phambu[1], Bashiyar Almarwani [1], Arlette M. Garcia [1], Nafisa S. Hamza[1], Amira Muhsen[2], Jacqueline E. Baidoo[2], and Anderson Sunda-Meya[2*]*

[1]Department of Chemistry, Tennessee State University, Nashville, TN 37209, USA

[2]Department of Physics and Engineering, Xavier University of Louisiana, New Orleans, LA 70125, USA

Corresponding Authors

*Anderson Sunda-Meya, asundame@xula.edu

* Nsoki Phambu, nphambu@tnstate.edu;

KEYWORDS

Antimicrobial Peptides structure; Antimicrobial Peptides stability; $(RW)_n$ Self-assembly; Peptide chain length effect.

ABSTRACT

Three peptides containing $(RW)_n$-NH_2 units (where n = 4, 6, and 8) have been chosen to study the effect of the chain length on the structure and stability of the peptide using Fourier Transform infrared (FTIR), scanning electron microscopy (SEM), thermogravimetric analysis (TGA), and differential scanning calorimetry (DSC) techniques. Their interactions with *Escherichia Coli* (*E. coli*) membrane mimetic vesicles are discussed. Infrared results indicate that addition of $(RW)_n$-NH_2 units increases intermolecular H bonds with antiparallel orientation. TGA and DSC results reveal that $(RW)_6$-NH_2 shows the optimal chain length in terms of stability and all three peptides show a preferential interaction with one of the anionic lipids in *E. coli* membranes. SEM images of $(RW)_4$-NH_2 present large aggregates while those of $(RW)_6$-NH_2 and $(RW)_8$-NH_2 present layers of sheet-like structure. In the presence of model membranes, $(RW)_n$-NH_2 show fibrillar peptide superstructures. This study suggests that repeating structures of $(RW)_n$-NH_2 promotes lateral assembly.

1. INTRODUCTION

Antimicrobial peptides (AMPs) are prospective antibiotics with a broad spectrum of activities against gram-negative and gram-positive bacteria, including antibiotic-resistant strains and some fungi, viruses, and parasites[1], but their killing mechanism is still open to debate[2]. The class of antimicrobial peptides containing $(RW)_n$-NH_2 units have been extensively studied[3–7]. The side chains R and W appear in many AMPs, but the effect of the chain length and composition on antimicrobial activity is not well understood. It is reported that the spatial position and arrangement of tryptophanes affect membrane-active peptide adsorption and activity[8–11] and tryptophanes have been observed to modulate hydrophobic mismatches to maintain peptide stability and activity in lipid bilayer membranes[12]. Peptides including positively charged amino

acids have been found to self-assemble and many studies have been devoted to the self-assembly process of peptides[13–21]. There is still no consensus on what controls and limits the size of high-order assemblies formed by repeating structures in peptide fibers[22].

Liu et al.[3] investigated the effect of length in antimicrobial peptides of the (RW)n series (n = 1-5). They found that the antimicrobial activity of the peptides increases with the chain length, and $(RW)_3$ showed the optimal chain length in terms of the efficacy of synthesis and selectivity as evaluated by the hemolytic index. Chen et al.[4] who also investigated the antibacterial activity of short hydrophobic and basic-rich peptides found that $(RW)_3$ had a good antimicrobial activity but was less active than the longer derivatives.

Based on the findings of Liu et al.[3] and Chen et al.[4], we decided to explore the effect of length in antimicrobial peptides of the (RW)n series for n >5. Because $(RW)_3$ showed the optimal chain length in terms of the efficacy of synthesis and selectivity, we chose the known $(RW)_4$-NH_2 as our reference to assess the effect of adding $(RW)_n$-NH_2 units. Doubling the number of (RW)n-NH_2 units leads to $(RW)_8$-NH_2. However, given that short peptides are preferred for their cost-effectiveness, we chose $(RW)_6$-NH_2 instead of any other $(RW)_n$-NH_2 with n>10.

We describe and compare the structure and stability of the peptides $(RW)_4$-NH_2, $(RW)_6$-NH_2, and $(RW)_8$-NH_2 in the dried state[11] and examine their interactions with *E. coli* mimicking cell membranes. Studies on the perturbations of the bilayers induced by peptides have been restricted to the effects of peptides on single or binary phospholipids[23–25]. We report on the perturbations of the peptides on bilayers of a very challenging model membrane that is a ternary mixture of lipids mimicking *E. coli* membranes[26]. Vibrational, thermogravimetric and imaging techniques are used in a complementary way to gain insights into the structure and stability of the samples.

2. EXPERIMENTAL SECTION

2.1. Materials

Dimyristoylphosphotidylethanolamine (DPPE), Dimyristoylglycerophosphorylglycerol (DPPG), and cardiolipin (CL) were purchased from Avanti Polar Lipid Inc. and used without further purification. The peptides (RW)n-NH_2 were obtained from GenScript (>97 % purity) and used as received.

2.2. *Escherichia Coli* membrane mimetic vesicles preparation.

The mixture of lipids used to mimic *E. coli* membrane composition is that used by Wei-Chin et al. [26], which is CL:DPPG:DPPE 1:5:15 (mol/mol/mol). The solid phases were obtained using two different concentration of peptide. $(RW)_n$ with the lipid mixture giving the $(RW)_n$:CL:DPPG:DPPE complex with the respective molar ratios 1:1:5:15 is called $(RW)_n$ - *E. coli* complex at high peptide concentration. (RW)n with the lipid mixture giving the (RW)n:CL:DPPG:DPPE complex with the respective molar ratios 0.02:1:5:15 is called (RW)n - *E. coli* complex at low peptide concentration. Vesicles were prepared using pure CL, DPPG, and DPPE powders.

The appropriate amount of dried lipid was weighed out and dissolved in chloroform and vortex for 5 minutes. The samples were dried under a stream of nitrogen gas for 6 hours and under vacuum overnight. A thin lipid film was formed on the wall of the vial. The thin lipid film was then hydrated with water at physiological pH to a total lipid concentration of 10μM. Small Unilamellar Vesicles (SUVs) were prepared by sonification of the milky lipid suspension using a Sonic Dismembrator Ultrasonic Processor (Model FB-50 including a standard 1/8" diameter microtip, in titanium alloy) from Fisher Scientific for about an hour in an ice bath until the solution became transparent. Stock solutions of $(RW)_n$ with a defined concentration were also

prepared. For peptide binding experiments, an appropriate volume of $(RW)_n$ was mixed to an appropriate volume of *E. coli* vesicles to make up the different solutions with different proportions of *E. coli* vesicles. Preparation of solid phases: we prepared $(RW)_n$ and their complexes with E.coli vesicles under the form of solids by drying a certain volume of a solution of interest. A vacuum apparatus FreeZone 6 from LABCONCO was used to obtain the freeze-dried samples. To avoid a plethora of variables such as organic solvent, incubation time and buffer, we kept our working conditions at the minimum, using double deionized water at physiological pH.

2.3. Characterization.

Infrared spectroscopy. Infrared spectra were obtained using a Fourier Transform instrument (Thermo Scientific iS10) equipped with a single reflection Ge attenuated total reflectance accessory. Solid samples were used. The change in vibration modes of (RW)n with and without the lipid mixture was then monitored. The spectra were recorded at room temperature between 4000 and 600 cm^{-1} at 4 cm^{-1} resolution and 64 scans were accumulated. Routine smoothing and normalization were applied to all the infrared spectra[27–29]. *Determination of the secondary structure.* The determination of the secondary structure from infrared spectra shows a matter of concern[29]. This is because the bands characteristic of amide I vibration are broad. In this case, a curve fitting treatment was carried out to estimate quantitatively the relative proportion of each component representing each type of secondary structure. FTIR spectra of (RW)n with and without lipid were recorded and used in this study[29,30]. First, the FTIR spectra were normalized. Then a linear baseline was used between 1700 and 1600 cm^{-1}, and a FT self-deconvolution was applied. The frequencies, the number of peaks to be fitted and the half width (15 cm^{-1}) of each peak to start a least square iterative curve fitting procedure, were obtained from the second

derivative of the original FTIR spectra. Then the deconvolution of the amide I band was performed with OMNIC Software (Thermo Fisher Scientific, Waltham, MA), and analyzed as a sum of Gaussian curves, with consecutive optimization of amplitudes, band positions, half-widths, and Gaussian composition of individual bands. The amount of each secondary structure element is given in percentage terms, by dividing the area of one amide I band component by the area of the sum of all amide band component areas. We assigned the types of secondary structures based on the data found in the literature[29–32]. *Thermogravimetric analysis (TGA) and Differential Scanning calorimetry (DSC).* Thermal stability and phase transitions of (RW)n and their complexes were recorded by Thermogravimetric Analysis (TGA)[33–35] and Differential Scanning Calorimetry (DSC)[8,34–36] with a LINSEIS STA PT1600 instrument. This instrument determines simultaneous changes (in a single run) of mass and caloric reactions of a sample. The instrument performs tests from ultrahigh vacuum 10^{-4} mbar to 5 bar over pressure. Samples weighing 4-6 mg were put in an aluminum pan and an empty pan was used as a reference. Investigations were performed between room temperature and 700^{o}C with a heating rate of 10^{o}C per minute. At this heating rate of 10^{o}C per minute, the degradation of the samples was reduced. Transition parameters were obtained with incorporate software[37,38]. The aliquots from the same freeze-dried samples are used for infrared, SEM, TGA and DSC. *Scanning electron microscopy (SEM).* The SEM images were obtained in a S4800 field emission scanning electron microscope (SEM) (Hitachi High Technologies America Inc., Gaithersburg, MD). All samples were gold sputter-coated at 2.0 mA for 1 min (K550X Sputter Coater, Quorum Technologies Ltd., West Sussex, UK). An accelerating voltage of 5 kV was used for all SEM observations.

3. RESULTS AND DISCUSSION

3.1. Structural analysis.

FTIR has been widely used to investigate the secondary structure of peptides and proteins[32,39–43]. The secondary structure of (RW)n series with and without *E. coli* membranes was examined by comparison of FTIR spectra at amide I (1700-1600 cm^{-1}) and amide II (1600-1500 cm^{-1}) regions that are characteristic of peptides. Figure 1 presents the original FTIR spectra of the (RW)n series and (RW)n series with *E. coli* membranes, at high peptide concentration. Figure 1S (in the supplemental material) displays the FTIR spectra of (RW)n series with *E. coli* membranes, at low peptide concentration in the supplemental materials.

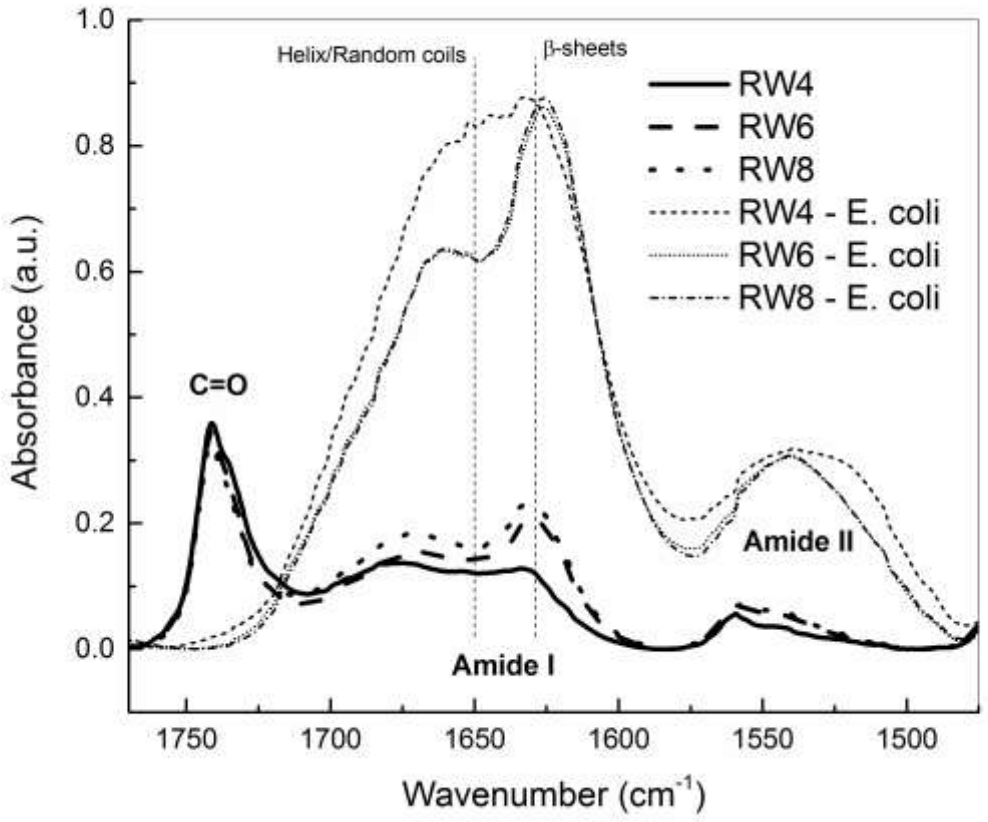

Figure 1. FTIR spectra of lyophilized samples of $(RW)_n$-NH_2 (obtained from a 10 μM aqueous solution at physiological pH) and (RW)n – E. coli complex at high peptide concentration (molar ratios 1:1:5:15).

From figure 1, one can observe that the FTIR spectrum of $(RW)_4$-NH_2 shows a broad symmetric peak containing an almost equal number of helix/random coils and sheet structures. Upon $(RW)_n$ addition, there is an obvious change in the profiles of the FTIR spectra of $(RW)_6$-NH_2 and $(RW)_8$-NH_2. Their peaks are still broad but completely dissymmetric, suggesting a concomitant increase in the sheet content and decrease in helix/random coils structures. The increase in sheet content is also observed in the FTIR spectra of the (RW)n-*E. coli* complexes (figures 1 and 1S). These infrared bands are so broad that it is difficult to determine the secondary structure of the peptide.

Since the amide I regions consist of broad bands, it was subject to curve-fitting in order to resolve the various subcomponents present in the amide I region[32,42]. The characteristic amide I peak described in the literature contains different secondary structures, including: strong intermolecular β-sheet (1622–1627 cm^{-1}), strong intramolecular β-sheet (1628–1637 cm^{-1}), weak β-sheet (1690–1703 cm^{-1}), random coils (1637–1644 cm^{-1}), α-helix (1645–1657 cm^{-1}), 3_{10}-helix (1658–1666 cm^{-1}), and turns (1668–1685 cm^{-1}). The conformation ranges above are based on the experimental data and assignments collected from various authors and evaluated by our team[32,40–44]. Table I summarizes the IR curve-fitting results obtained for all the samples. Figures 2S, 3S, and 4S in the supplemental materials display the infrared results of the curve-fitted amide I regions of $(RW)_4$, $(RW)_6$, and $(RW)_8$, respectively.

Table I. Percentage of secondary structures in RWn-NH_2 samples with and without E. coli model membranes (all calculated secondary structure fractions have a same unit (wt %) with a 2 wt % error bar).

Secondary structure	Extremes of band positions	RW4	RW6	RW8	RW4-E. coli	RW6-E. coli	RW8-E. coli
α-helix	1645-1657	16	19				
3_{10}-helix	1658-1664	17	18	28		27	
Intermolecular β-sheet	1622-1627		23	30			
Intramolecular β-sheet	1628-1637	26	19		44	48	49
Anti-parallel β-sheet	1686-1703	5	8	8			
Turns	1665-1685	18	13	13	56	25	51
Random coils	1638-1644	18		21			
Sheet/Helix		0.941	1.378	1.172			

The results of quantitative analysis of peptide conformation (table I) shows that $(RW)_4$-NH_2 consists of a mixture of helix (34%), β-sheet (32%), β-turns (16%), and random coils (18%) structures. $(RW)_6$-NH_2 and $(RW)_8$-NH_2 are also composed of a mixture of the same conformations with different proportions. The total amount of helix and sheet structures is 37% and 51%, respectively, in $(RW)_6$-NH_2, and the total amount of helix and sheet is 29% and 34%, respectively, in $(RW)_8$-NH_2. Addition of (RW)n-NH_2 units results in an increase in (a) intermolecular H bonds with antiparallel orientation, (b) sheet/helix content ratio, and (c) 3_{10}-helix structures to some extent. This increase in sheet is consistent with the general behavior of peptides composed of alternating aromatic/hydrophobic (W) and positively charged (R) amino acids. The presence of aromatic tryptophan has been found to increase the strength of the β-sheet association via π-π stacking interactions[43,45]. The β-sheet content is in the order $(RW)_4$<$(RW)_8$<$(RW)_6$. Knowing that the secondary structures of (RW)n series are different, we aimed to monitor if these differences translate to a different impact on membrane interfaces.

In the presence of *E. coli* membranes, the contents of α-helix and random coils of $(RW)_4$ and $(RW)_8$ have disappeared. The curve-fitting data (table I) and the profiles of the FTIR curves (figures 1 and 1S) suggest that random coils structures are converted to turns in the presence of *E. coli* membranes, leading to a large increase in turns content and a dramatic decrease in helix in $(RW)_4$ and $(RW)_8$; $(RW)_6$ has the lowest content in turns, but a significant content in helix remains. The intermolecular sheets are changed to intramolecular sheets in all the cases. These changes suggest a strong interaction between (RW)n and *E. coli* model membranes through a conformational change. When a very low amount of peptide is added to *E. coli* membrane, the changes in the corresponding FTIR spectra are small (Figure 1S), but the changes in the corresponding SEM images (figure 2 G, H, I) are very significant as seen in the next section. The intensity of the carbonyl peak of the lipid at around 1740 cm^{-1} (figures 1 and 1S) remains unchanged in position and intensity, suggesting that this carbonyl group is not involved in the bonding.

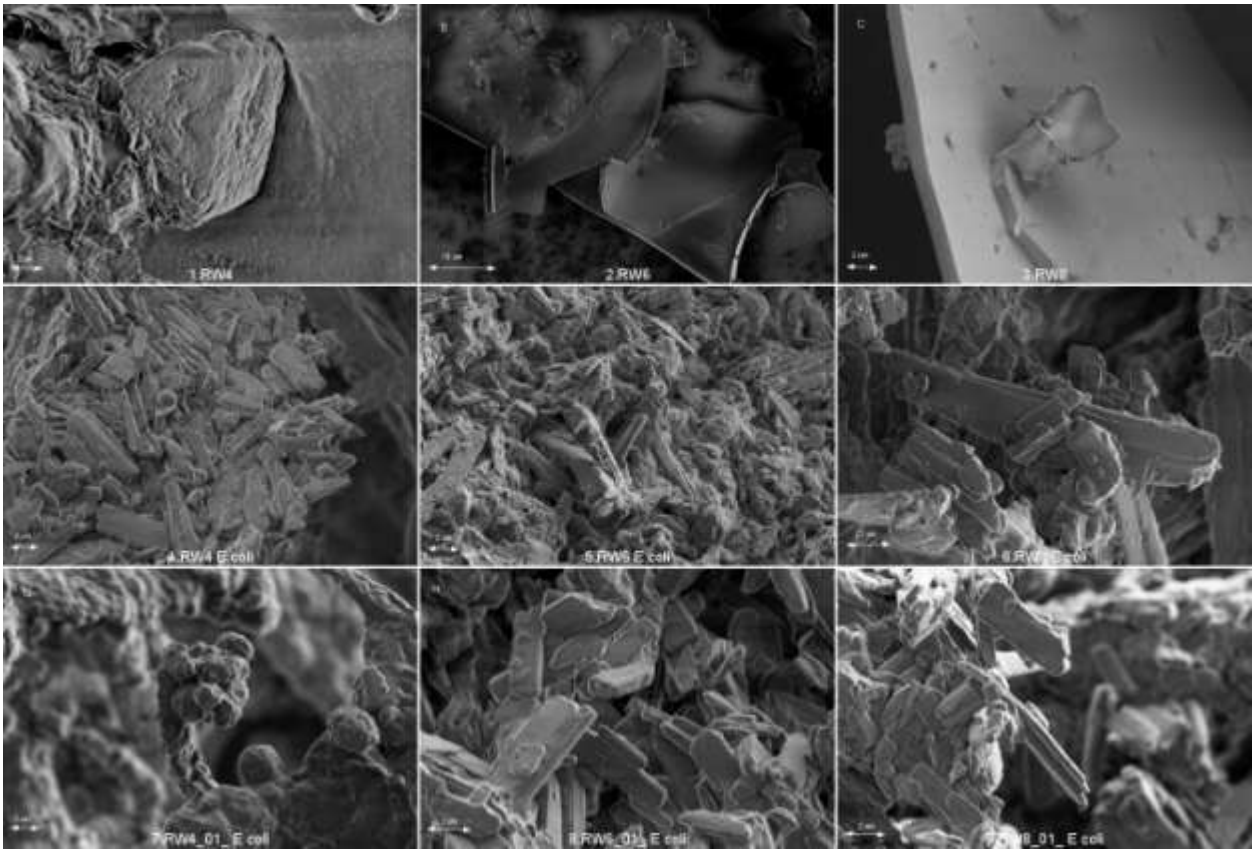

Figure 2. SEM images of lyophilized samples of (RW)n-NH_2 obtained from a 10 μM aqueous solution at physiological pH (panel A, B, C), of lyophilized samples of (RW)n -E. coli complex at high peptide concentration (panels D,E,F), and of lyophilized samples of (RW)n -E. coli complex at low peptide concentration (panels G,H,I) .

3.2. Ultrastructural analysis.

SEM was used to visualize the effect of the chain length addition. The SEM images shown in panels A, B, and C of figure 2 provide a strong evidence that adding (RW)n units promotes lateral assembly. $(RW)_4$ sample (figure 2A) presents large aggregates including multiple stacked thin sheets wrapped on an amorphous matrix. No obvious fibrils appear. The presence of a significant amount of sheets and random coils structures in $(RW)_4$ may explain these features. SEM images (panels B and C) show that $(RW)_6$ and $(RW)_8$ present mostly dense layers of sheet

like structures of a few micron thickness[46]. The average measured thickness of layers of sheet is ~1.2 μm, and the surface is smooth and homogeneous. This can be explained by the fact that $(RW)_6$ and $(RW)_8$ have probably reached the minimum amount of sheets required to form an extended network, a lateral assembly made up of layers of sheets[41–48]. The surface of the layers is also smooth and homogeneous.

The SEM images in panels D, E, and F of figure 2 show the interaction of (RW)n with *E. coli* membrane mimetic vesicles at high peptide concentration. All three complexes reveal the presence of ribbons (plates) mostly with some spherical particles. The spherical particles are probably made of turns while ribbons are made of sheets[19,39,43,47], in agreement with the infrared data in table I.

At low peptide concentration, some really striking features appear especially in the case of $(RW)_4$. $(RW)_4$ reveals the presence of spherical interconnected micro clusters, with a diameter range of approximately 3-5 μm (figure 2 panel G). These SEM images resemble the images described by Gribbon et al.[49] and Aronsson et al.[48] showing fibrous peptide superstructures. The SEM images corroborate the results of infrared analysis (table I), suggesting that random coils and helix structures of (RW)4 are converted into turns in the presence of *E. coli* membranes to produce spherical clusters. $(RW)_6$ and $(RW)_8$ (figure 2 panels H,I) present mostly thickened and ordered fiber-like ribbons/plates with a thickness of a few nanometer sizes[46]. The ribbons/plates have a rectangular-like shape. The average length, width, and height of the plates are 7, 2, and 0.2 μm. SEM images suggest that (RW)n disrupt *E. coli* mimicking membranes by forming superstructures. Comparison of panels D, E, F and G, H, I of figure 2 reveals that (RW)n have a different effect on *E. coli* vesicles and these effects depend on peptide concentration.

3.3. Thermal analysis

TGA and DSC were used to study the effects of adding (RW)n units on the thermal stability of the resulting samples and evaluate the moisture content of the samples. The level of hydration has been found to affect the thermal stability of proteins[50,51]. Water molecules may form a bridge between hydrophobic molecules leading to an extended network[50]. Also, Liberato et al.[32] have found that water intercalated into the matrix of the assemblies would stimulate the formation of H-bonds, which would account for the self-assembly of larger structures[32].

In general, from the TGA profiles, there are three main regimes of weight loss. The first one between room temperature and 200^{o}C corresponds to the loss of weakly bound surface and interlayer water. The second one between 200^{o}C and 450^{o}C corresponds to the breaking of the bonds. This complex event includes decarboxylation, deamination, desulphyration, dephosphorylation, etc…). The third endothermic event beyond 450^{o}C consists of complete decomposition of the sample[36,52]. We keep in mind that complexes are most stable when a smaller loss of mass occurs over a given temperature range[36].

Figures 3 and 4 present the TGA and DSC profiles of (RW)n series, respectively. At 50% weight loss, figure 3 reveals that $(RW)_4$ loses 50% of its mass at a lower temperature than $(RW)_8$, and $(RW)_8$ loses 50% of its mass at a lower temperature than $(RW)_6$; thus the thermal stability is in the order $(RW)_6$>$(RW)_8$>$(RW)_4$. This order of thermal stability is in agreement with the order of β-sheet content suggested by the infrared data. It has been suggested the sheets are more stable than helix[50]. From figure 4, the energy required to remove water molecules (between room temperature and 250^{o}C) is roughly 22 J/g, 535 J/g, and 282 J/g for $(RW)_4$, $(RW)_6$, and $(RW)_8$, respectively. This is suggesting that water content is in the order $(RW)_6$>$(RW)_8$>$(RW)_4$. Water molecules are the bridges requires to link different arginine

residues to form extended network leading to large sheets like-structure seen in SEM images of $(RW)_6$ and $(RW)_8$[32].

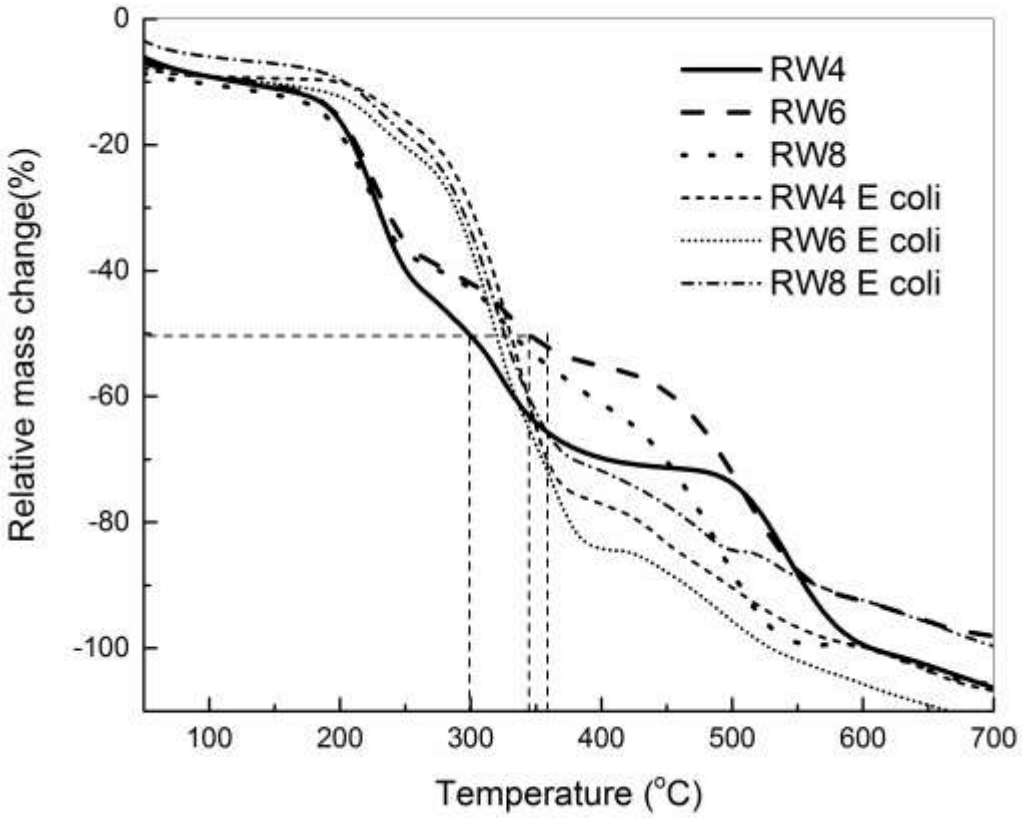

Figure 3. TGA curves for lyophilized samples of (RW)n-NH_2 (obtained from a 10 μM aqueous solution at physiological pH) and (RW)n – E. coli complex at high peptide concentration (molar ratios 1:1:5:15).

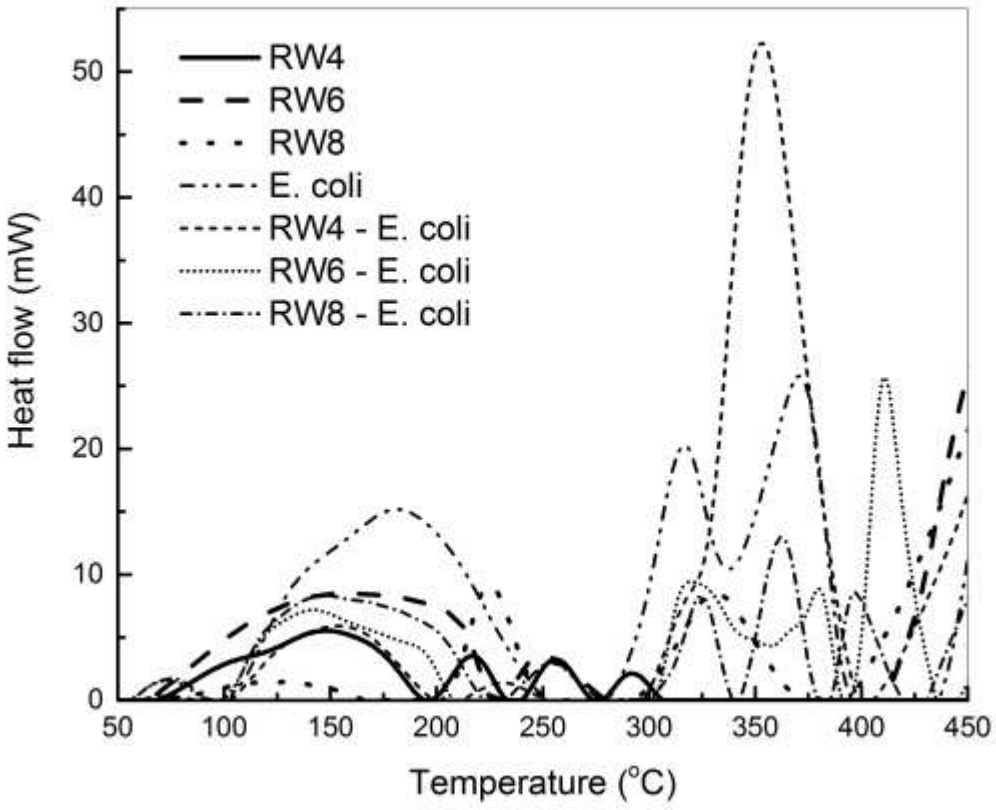

Figure 4. DSC thermograms for lyophilized samples of (RW)n-NH_2 (obtained from a 10 μM aqueous solution at physiological pH) and (RW)n -E. coli complex at high peptide concentration (molar ratios 1:1:5:15).

In the presence of *E. coli* model membranes, figure 3 reveals that the order of thermal stability of complex samples is $(RW)_4$-*E. coli* > $(RW)_8$-*E. coli* > $(RW)_6$-*E. coli*. This order is also in agreement with the IR results suggesting that $(RW)_4$ contains more unordered structures than $(RW)_6$ and $(RW)_8$, and these random coils structures of $(RW)_4$ are converted mostly into turns in the presence of *E. coli* model membranes. This feature may explain why $(RW)_4$ is more reactive

than $(RW)_6$ and $(RW)_8$. The random coils structures of $(RW)_6$ and $(RW)_8$ are mostly converted into a mixture of sheet and helix structures.

To verify whether the peptides could discriminate between the components of the ternary mixture of phospholipids mimicking *E. coli* membranes, we compared the 250-400^{o}C regions where the lipids appear. Figure 4 presents the DSC profile of *E. coli* mimicking vesicles, showing a broad and asymmetric peak with an enthalpy change of about 909 J/g corresponding to the breaking of the H and intermolecular bonds of the lipid mixture. The asymmetric property of the peak may be related to the non-ideal behavior of the ternary lipid mixture (CL:DPPG:DPPE). The low and high temperature peaks have almost the same amplitude.

This peak is differently and dramatically affected by the presence of (RW)n. The results of low and high peptide concentrations are similar. In the presence of $(RW)_4$, the low temperature peak decreases in amplitude while the high temperature peak becomes higher and sharper, and completely dissymmetric. These data suggest that $(RW)_4$ discriminates between the lipid components; the low temperature peak corresponds to the peptide-poor domain and the high temperature peak to the peptide-rich domain, a phenomenon already seen in the literature[11,38]. Also, the total enthalpy has increased from 924 J/g to 2036 J/g, suggesting a stabilizing effect of the model membranes by $(RW)_4$. In the presence of $(RW)_6$ and $(RW)_8$, the intensities of the peak of *E. coli* model membranes have also decreased and sometimes completely separated as seen in the case of $(RW)_8$-E.coli complex, and a new peak maximum has appeared at around 420^{o}C. The total enthalpy in the selected region has decreased. The reduction of intensities suggests that $(RW)_6$ and $(RW)_8$ are able to recruit the negatively charged lipids, like $(RW)_4$. This is due to the presence of R residue, as the role of R residue in promoting anionic lipid clustering is well-known[11]. The reduction in total enthalpy points towards a destabilizing effect of the model

membrane by $(RW)_6$ and $(RW)_8$. Overall, the three peptides interact strongly but differently with *E. coli* mimicking membranes.

We suggest that the order of strength of the complex is $(RW)_4$-E. coli > $(RW)_8$-E. coli > $(RW)_6$-E. coli, in agreement with the TGA and IR data. In addition, the combination of the four techniques used herein has revealed the self-assembly behavior of the (RW)n peptides and the resultant superstructures. With respect to $(RW)_4$, the increased stability of $(RW)_6$ and $(RW)_8$ peptides may be due to the increase in net positive charge due to the increased length, leading to a finer balance between π-π stacking of tryptophan residues and steric effects. From the point of view of mechanism of interaction, this study suggests that the negative region of membrane is the target of these antimicrobial peptides of the (RW)n series (n = 4,6,8) through the presence of arginine residues. This preferential membrane interaction of (RW)n peptides may provide an insight into the studies of peptide and bacterial membrane interactions. The presence of a helical conformation in two helical tracts may also offer a new direction in the studies of fibrils in neurodegenerative diseases.

CONCLUSIONS

We have examined the effects of the chain length on the structure and stability of antimicrobial peptides of the (RW)n series using FTIR, SEM, TGA and DSC techniques. Addition of (RW)n-NH_2 units results in an increase in sheet/helix structure content ratio, 3_{10}-helix structures, and intermolecular H bonds with antiparallel orientation, promoting a lateral assembly. Vibrational data revealed a multiplicity of secondary structures corresponding to a multiplicity of peaks in TGA/DSC profiles related to various morphologies shown by SEM. We have established that peptides of the (RW)n series show a preferential interaction with one of the anionic lipids and are

able to disrupt the *E. coli* membrane. In one hand, the ability of (RW)n to form superstructures with *E. coli* model membranes seems to be a requirement for their antimicrobial activity. In the other hand, the ability of (RW)n series to form a fibrillar structure in solid state is similar to that of amyloid fibrils. Thus, the fibrillar morphology of peptides of the (RW)n series may be used as a model system to study the fibrillation process of many neurotoxic diseases causing amyloid fibrils. Finally, this approach may be useful in creating new materials in nanotechnology by self-assembly.

AUTHOR INFORMATION

Author Contributions

The manuscript was written through contributions of all authors. All authors have given approval to the final version of the manuscript.

ACKNOWLEDGMENTS

N.P. wants to express his deepest gratitude to Tennessee State University for the support.

This material is based upon work supported by the National Science Foundation Research Initiation Awards and HBCU-UP under Grants No. 1411209 and 1036147.

REFERENCES

(1) Hancock, R. E. W. Host Defence (Cationic) Peptides: What Is Their Future Clinical Potential? *Drugs* **1999**, *57* (4), 469–473.
(2) Nowotarska, S. W.; Nowotarski, K. J.; Friedman, M.; Situ, and C. Effect of Structure on the Interactions between Five Natural Antimicrobial Compounds and Phospholipids of Bacterial Cell Membrane on Model Monolayers. *Molecules* **2014**, *19*, 7497–7515.
(3) Liu, Z.; Young, A. W.; Hu, P.; Rice, A. J.; Zhou, C.; Zhang, Y.; Kallenbach, N. Length Effects in Antimicrobial Peptides of the (RW)n Series. *Antimicrob Agents Chemother* **2007**, *51*, 597–603.
(4) Chen, P.-W.; Shyu, C.-L.; Mao, and F. C. Antibacterial Activity of Short Hydrophobic and Basic-Rich Peptides. *Am. J. Vet. Res.* **2003**, *64* (9), 1088–1092.
(5) Vogel, H. J. Interactions of the Antimicrobial Peptide Ac-FRWWHR-NH2 with Model Membrane Systems and Bacterial Cells. *J Pept. Res* **2005**, *65*, 491–501.
(6) Jing, W.; Hunter, H. N.; Hagel, J.; Vogel, H. J. The Structure of the Antimicrobial Peptide Ac-RRWWRF-NH2 Bound to Micelles and Its Interactions with Phospholipid Bilayers. *J Pept Res* **2003**, *61* (5), 219–29.
(7) Chan, D. I.; Prenner, E. J.; Vogel, H. J. Tryptohan- and Arginine-Rich Antimicrobial Peptides: Structure and Mechanisms of Action. *Biochim Biophys Acta* **2006**, 1758–1184.
(8) Li, G.; Huang, Y.; and Yuxin Chen, Q. F. Tryptophan as a Probe to Study the Anticancer Mechanism of Action and Specificity of α-Helical Anticancer Peptides. *Molecules* **2014**, *19*, 12224–12241.
(9) Schiopu, I.; Mereuta, L.; Apetrei, A.; Park, Y.; Hahm, K. S.; Luchian, T. The Role of Tryptophan Spatial Arrangement for Antimicrobial-Derived, Membrane-Active Peptides Adsorption and Activity. *Mol Biosyst 2012* (8), 2860–2863.
(10) Rekdal, O.; Haug, B. E.; Kalaaji, M.; Hunter, H. N.; Lindin, I.; Israelsson, I.; Solstad, T.; Yang, N.; Brandl, M.; Mantzilas, D. Relative Spatial Positions of Tryptophan and Cationic Residues in Helical Membrane-Active Peptides Determine Their Cytotoxicity. *J Biol Chem* **2012**, *287*, 233–244.
(11) Wadhwani, P.; Epand, R. F.; Heidenreich, N.; Bu¨rck, J.; Ulrich, A. S.; Epand, and R. M. Membrane-Active Peptides and the Clustering of Anionic Lipids. *Biophys. J.* **2012**, *103*, 265–274.
(12) De Jesus, A. J.; Allen, T. W. The Role of Tryptophan Side Chains in Membrane Protein Anchoring and Hydrophobic Mismatch. *Biochim Biophys Acta* **2013**, *1828*, 864–876.
(13) Popielski, L.; and Xiao Hu, N. R. Comparative Study of Ultrasonication-Induced and Naturally Self-Assembled Silk Fibroin-Wool Keratin Hydrogel Biomaterials. *Int J Mol Sci* **2016**, *17*, 1497.
(14) Bakota, E. L.; Sensoy, O.; Ozgur, B.; Sayar, M.; Hartgerink, and J. D. Self-Assembling Multidomain Peptide Fibers with Aromatic Cores. *Biomacromolecules* **2013**, 14–1370.
(15) Beytullah. Ozgur and Mehmet Sayar. Assembly of Triblock Amphiphilic Peptides into One-Dimensional Aggregates and Network Formation. *J. Phys. Chem. B* **2016**, *120* (39), 10243–10257.
(16) Vanhalle, M.; Corneillie, S.; Smet, M.; Puyvelde, P. V.; Goderis, and B. Poly(alanine): Structure and Stability of the D and L- Enantiomers. *Biomacromolecules* **2016**, *17*, 183–191.
(17) Vasconcelos, A.; Freddi, G.; Cavaco-Paulo, A. Biodegradable Materials Based on Silk Fibroin and Keratin. *Biomacromolecules 2008* (9), 1299–1305.

(18) Hu, X.; Lu, Q.; Sun, L.; Cebe, P.; Wang, X.; Zhang, X.; Kaplan, D. L. Biomaterials from Ultrasonication-Induced Silk Fibroin−Hyaluronic Acid Hydrogels. *Biomacromolecules* **2010**, *11* (11), 3178–3188.
(19) Handelman, A.; Kuritz, N.; Natan, A.; Rosenman, and G. Reconstructive Phase Transition in Ultrashort Peptide Nanostructures and Induced Visible Photoluminescence. *Langmuir* **2016**, *32* (12), 2847–2862.
(20) Surmacz-Chwedoruk, W.; Malka, I.; Bożycki, Ł.; Nieznańska, H.; Dzwolak, W. On the Heat Stability of Amyloid-Based Biological Activity: Insights from Thermal Degradation of Insulin Fibrils. *PLoS ONE* **2014**, *9* (1), 86320.
(21) Tsiourvas, D. Athena Tsetsekou, Maria-Izoldi Kammenou, Nikos Boukos. Biomimetic Synthesis of Ribbon-like Hydroxyapatite Employing poly(L-Arginine). *Mater. Sci. Eng. C* **2016**, *58*, 1225–1231.
(22) Pandya, M. J.; Spooner, G. M.; Sunde, M.; Thorpe, J. R.; Rodger, A.; Woolfson, D. N. Sticky-End Assembly of a Designed Peptide Fiber Provides Insight into Protein Fibrillogenesis †. *Biochemistry* **2000**, *39* (30), 8728–8734.
(23) Alves, I. D.; Correia, I.; Jiao, C. Y. Emmanuelle Sachon, Sandrine Sagan, Solange Lavielle, Gordon Tollind and Gerard Chassaing. The Interaction of Cell-Penetrating Peptides with Lipid Model Systems and Subsequent Lipid Reorganization: Thermodynamic and Structural Characterization. *J Pept Sci* **2009**, *15*, 200–209.
(24) Joanne, P.; Galanth, C.; Goasdoué, N.; Nicolas, P.; Sagan, S.; Lavielle, S.; Chassaing, G.; Amri, C. E.; Alves, I. D. Lipid Reorganization Induced by Membrane-Active Peptides Probed Using Differential Scanning Calorimetry. *Biochim. Biophys. Acta* **2009**, *1788*, 1772–1781.
(25) van der Wel, P. C. A.; Pott, T.; Morein, S.; Greathouse, D. V.; Koeppe, R. E.; Killian, and J. A. Tryptophan-Anchored Transmembrane Peptides Promote Formation of Nonlamellar Phases in Phosphatidylethanolamine Model Membranes in a Mismatch-Dependent Manner. *Biochemistry* **2000**, *39*, 3124–3133.
(26) Wei-Chin. Hung and Ming-Tao Lee. The Interaction of Melittin with E. Coli Membrane: The Role of Cardiolipin. *Chin. J. Phys.* **2006**, *44* (2), 137–149.
(27) Benesch, M. G.; Mannock, D. A.; Lewis, R. N.; McElhaney, R. N. A Calorimetric and Spectroscopic Comparison of the Effects of Lathosterol and Cholesterol on the Thermotropic Phase Behavior and Organization of Dipalmitoylphosphatidylcholine Bilayer Membranes. Biochemistry. **2011**, *50* (46), 9982–9997.
(28) McMullen, T. P. W.; Lewis, R. N. A. H.; McElhaney, R. N. Calorimetric and Spectroscopic Studies of the Effects of Cholesterol on the Thermotropic Phase Behavior and Organization of a Homologous Series of Linear Saturated Phosphatidylethanolamine Bilayers. *Biochim. Biophys. Acta* **1999**, *1416*, 119–134.
(29) Jackson, M.; Mantsch, H. H. The Use and Misuse of FTIR Spectroscopy in the Determination of Protein Structure. *Crit Rev Biochem Mol Biol 1995* (30), 95–120.
(30) Deshayes, S.; Heitz, A.; Morris, M. C.; Charnet, P.; Divita, G.; Heitz, F. Insight into the Mechanism of Internalization of the Cell-Penetrating Carrier Peptide Pep-1 through Conformational Analysis. *Biochemistry* **2004**, *17* (43), 1449–57.
(31) Frias, M.; Benesch, M. G. K.; Lewis, R. N. A. H.; McElhaney, R. N. On the Miscibility of Cardiolipin with 1,2-Diacyl Phosphoglycerides: Binary Mixtures of Dimyristoylphosphatidylethanolamine and Tetramyristoylcardiolipin. *Biochim. Biophys. Acta BBA - Biomembr.* **2011**, *1808* (3), 774–783.

(32) Liberato, L. M. S.; KogikoskiJr., S.; Silva, E. R.; Coutinho-Neto, M. D.; Scott, L. P. B.; Silva, R. H.; OliveiraJr., V. X.; Ando, R. A.; A, and W. Alves. Self-Assembly of Arg–Phe Nanostructures via the Solid–Vapor Phase Method. *J Phys Chem B* **2013**, *117* (3), 733–740.
(33) Hu, X.; and Peggy Cebe, D. K. Thermal Analysis of Protein-Mettalic Ion Systems. *J Therm Anal Calorim* **2009**, *96*, 827–834.
(34) Tian, F.; Samir Sane, J. H. Rytting. Calorimetric Investigation of Protein/Amino Acid Interactions in the Solid State. *Int. J. Pharm.* **2006**, *310*, 175–186.
(35) and G. Marrosu, F. R. Thermal Analysis of Some α-Amino Acids Using Simultaneous TG-DSC Apparatus. The Use of Dynamic Thermogravimetry to Study the Chemical Kinetics of Solid State Decomposition. *Thermochim. Acta* **1990**, *171* (24), 15–29.
(36) Gorinstein, S. Thermogravimetric Study of the Stability under Heat of Iron-Protein Complexes. *J. Agric. Food Chem.* **1975**, *23* (1), 45–47.
(37) Interaction of Alpha-Melanocyte Stimulating Hormone with Binary Phospholipid Membranes: Structural Changes and Relevance of Phase Behavior. *Biophys J* **2001**, *80* (5), 2273–83.
(38) Misiewicz, J.; Afonin, S.; Ulrich, A. S. *Control and role of pH in peptide-lipid interactions in oriented membrane samples. Biochimica et Biophysica Acta 1848*; 2015.
(39) Zhou, S.; Peng, H.; Yu, X.; Zheng, X.; Cui, W.; Zhang, Z.; Li, X.; Wang, J.; Weng, J.; Jia, W.; Li, and F. Preparation and Characterization of a Novel Electrospun Spider Silk Fibroin/Poly(D,L-Lactide) Composite Fiber. *J Phys Chem B* **2008**, *112* (36), 11209–11216.
(40) Du, Z. Yi-Xin Guan, Shan-Jing Yao, Zi-Qiang Zhu. Supercritical Fluid Assisted Atomization Introduced by an Enhanced Mixer for Micronization of Lysozyme: Particle Morphology, Size and Protein Stability. *Int. J. Pharm.* **2011**, *421*, 258–268.
(41) Yamaoki, Y.; Imamura, H.; Fulara, A.; Wójcik, S.; Bożycki, Ł.; Kato, M.; A, T. Keiderling, and Wojciech Dzwolak. An FTIR Study on Packing Defects in Mixed β-Aggregates of Poly(L-Glutamic Acid) and Poly(D-Glutamic Acid): A High-Pressure Rescue from a Kinetic Trap. *J Phys Chem B* **2012**, *116* (17), 5172–5178.
(42) Kennedy, D. F.; Crisma, M.; Toniolo, C.; Chapman, and D. Studies of Peptides Forming 310- and α-Helices and β-Bend Ribbon Structures in Organic Solution and in Model Biomembranes by Fourier Transform Infrared Spectroscopy. *Biochemistry* **1991**, *30* (6541–6548), 6541.
(43) Dutta, A.; Kar, S.; Fröhlich, R. Pradyot Koley, and Animesh Pramanik. Studies of the β-Sheet Mediated Self-Assembly of Designed Synthetic Peptides of General Formula PhCO-Gly-Xx-OCH2Ph and the Possible Role of Aromatic π-π Interactions in the Self-Assembly. *ARKIVOC* **2009**, 247–259.
(44) Fulara, A.; Lakhani, A.; Wojcik, S.; Nieznanska, H.; Keiderling, T. A.; Dzwolak, and W. Spiral Superstructures of Amyloid-Like Fibrils of Polyglutamic Acid: An Infrared Absorption and Vibrational Circular Dichroism Study. *J Phys Chem B* **2011**, *115*, 11010–11016.
(45) Han, S.; Lee, M.; Lim, Y. Cell-Penetrating Cross-β Peptide Assemblies with Controlled Biodegradable Properties. *Biomacromolecules* **2017**, *18* (1), 27–35.
(46) Kar, S.; a. Kung-Wei Wu, I-Jui Hsu, Chi-Rung Lee and Yian Tai. Study of the Nano-Morphological Versatility by Self-Assembly of a Peptide Mimetic Molecule in Response to Physical and Chemical Stimuli. *Chem Commun* **2014**, *50*, 2638–2641.

(47) Saiki, M.; Honda, S.; Kawasaki, K.; Zhou, D.; Kaito, A. Takeo Konakahara and Hisayuki Morii.Higher-Order Molecular Packing in Amyloid-like Fibrils Constructed with Linear Arrangements of Hydrophobic and Hydrogen-Bonding Side-Chains. *J Mol Biol* **2005**, *348*, 983–998.
(48) Aronsson, C.; Selegård, R.; Aili, and D. Zinc-Triggered Hierarchical Self-Assembly of Fibrous Helix–Loop–Helix Peptide Superstructures for Controlled Encapsulation and Release. *Macromolecules* **2016**, *49* (18), 6997–7003.
(49) MagicWand: A Single, Designed Peptide That Assembles to Stable, Ordered R-Helical Fibers. *Biochemistry* **2008**, *47*, 10365–10371.
(50) Dandurand, J.; Samouillan, V.; Lacoste-Ferre, M. H.; Lacabanne, C.; B.Bochicchio, A. P. Conformational and Thermal Characterization of a Synthetic Peptidic Fragment Inspired from Human Tropoelastin: Signature of the Amyloid Fibers. *Pathol. Biol.* **2014**, *62*, 100–107.
(51) Jeevithan, E.; Jingyi, Z. Nanping Wang, Lan He, Bin Bao,Wenhui Wu. Physico-Chemical, Antioxidant and Intestinal Absorption Properties of Whale Shark Type-II Collagen Based on Its Solubility with Acid and Pepsin. *Process Biochem.* **2015**, *50*, 463–472.
(52) Fuentes, N. A. I.; Alegría, L.; Sandoval, C. Galder Kortabería, Arantxa Eceiza, Ligia Gargallo, Angel Leiva, Deodato Radić. Interactions in Blends of Dendronized Polymeric Nanocomposites with Some Common Drugs. *J Appl Polym Sci* **2015**, *132*, 42450–60.